Combustion and Flame 257 (2023) 113030

Contents lists available at ScienceDirect

Combustion and Flame

journal homepage: www.elsevier.com/locate/combustflame

Effect of radiation on laminar flame speed determination in spherically propagating NH_3-air, NH_3/CH_4-air and NH_3/H_2-air flames at normal temperature and pressure

Mahdi Faghih[a,*], Agustin Valera-Medina[b], Zheng Chen[c], Amin Paykani[d]

[a] School of Physics Engineering and Computer Science, University of Hertfordshire, Hatfield, AL10 9AB, UK
[b] Institute of Mechanical and Manufacturing Engineering, School of Engineering, Cardiff University, Cardiff, CF24 3AA, UK
[c] SKLTCS, Department of Mechanics and Engineering Science, College of Engineering, Peking University, Beijing 100871, China
[d] School of Engineering and Materials Science, Queen Mary University of London, E1 4NS, UK

ARTICLE INFO

Article history:
Received 28 November 2022
Revised 17 July 2023
Accepted 17 August 2023

Keywords:
Radiation
NH_3-air
NH_3/CH_4-air
NH_3/H_2-air
Laminar flame speed
Spherically propagating flame

ABSTRACT

The use of spherically propagating flames is common for measuring the laminar flame speed in NH_3-air, NH_3/CH_4-air and NH_3/H_2-air mixtures. However, the radiation-induced uncertainty in such mixtures has not been thoroughly investigated. Due to the low laminar flame speed of ammonia mixtures, it is anticipated that the radiation effect is considerable for such mixtures. This study aims to fill this gap by conducting numerical simulations using different chemical mechanisms and the adiabatic and optical thin radiation models to examine the effects of radiation on spherically propagating NH_3-air, NH_3/CH_4-air and NH_3/H_2-air flames. The simulations are performed for mixtures at normal temperature and pressure (T_u=298 K and P = 1 atm) and wide range of equivalence ratios. The radiation-induced uncertainty in spherical flames is quantified and compared to planar flames. The importance of the radiation-induced flow and thermal effects in spherical flames is compared between different mixtures and a correlation is developed to determine the radiation-corrected flame speed for spherical NH_3-air flames. Considering the radiation effect in NH_3-air, it was found that using different mechanisms results in considerable discrepancies in laminar flame speed determination. Some mechanisms showed that the radiation-induced flame speed in spherical flames was underpredicted by more than two times compared to planar flames, and the radiation-induced uncertainty for lean and rich spherically propagating NH_3-air flames exceeds 20%. However, the radiation-induced uncertainty at normal temperature and pressure in spherically propagating NH_3/CH_4-air and NH_3/H_2-air flames was less significant, not exceeding 11%. Finally, an updated correlation is proposed to determine the radiation-corrected flame speed for NH_3-air flames that can be directly used in spherical flame experiments measuring the laminar flame speed.

1. Introduction

Increase in global warming and climate change is predicted to have serious impacts on human health and the environment. Future propulsion and power generation technologies should use non-carbon energy sources combined with advanced high efficiency energy conversion devices to meet net-zero carbon emissions targeted by 2050. Ammonia (NH_3) has attracted much attention for combustion applications in recent years due to its established production, transportation, and storage infrastructure [1,2]. However, there are important challenges with NH_3 combustion including low laminar flame speed, low heating value, narrow flammability limit, and large NOx emissions, which should be overcome before widespread practical use [1]. To overcome these challenges, mixing NH_3 with more reactive fuels, such as hydrogen (H_2) and methane (CH_4), has been suggested [1].

There are numerous studies on the application of NH_3-air, NH_3/CH_4-air, and NH_3/H_2-air in gas turbines, boilers and internal combustion engines [3–7]. Different detailed chemical mechanisms have been developed to characterize ammonia blends combustion [4,8-11]. Among the experimental methods used to develop these chemical mechanisms, the use of spherically propagating flames (SPF) is the preferred option to measure the laminar flame speed (LFS) at engine relevant conditions, (i.e., at P = 20–50 atm and T_u = 700–800 K) [12]. Therefore, the SPF method has been popularly used to measure the LFS of ammonia-blends and to vali-

* Corresponding author.
E-mail address: m.faghih-abdollahi@herts.ac.uk (M. Faghih).

https://doi.org/10.1016/j.combustflame.2023.113030

date chemical mechanisms [10,13-17]. Chen [18] has shown that even for methane/air mixtures at normal temperature and pressure (NTP, T_u=298 K and $P = 1$), the maximum difference of reported unstretched laminar flame speed ($S_{u,0}$) exceeds 20% for $\phi \leq 0.9$ and $\phi \geq 1.2$. Consequently, accurate measurement of LFS is essential due to the low sensitivity of LFS to chemical kinetics [19].

Different factors including mixture preparation [19,20], ignition [21], buoyancy [22,23], instability [24,25], confinement [26,27], nonlinear stretch behavior [28], extrapolation [29], and radiation [30–32] induce uncertainty in SPF measurements. One of the main sources of uncertainty in SPF experiments is radiation [30,31,33,34], which is noticeable for mixtures with LFS below 10 cm/s [35]. Due to the relatively low LFS of NH_3-air NH_3/CH_4-air, and NH_3/H_2-air mixtures with low hydrogen contents, the importance of radiation-induced uncertainty seems to be considerable. However, relatively few studies have been performed to investigate radiation effect in ammonia blends. Nakamura and Shindo [36] used the optically thin model (OTM) [37] and CHEMKIN-PREMIX [38] package to study the radiation effect in steady planar freely propagating NH_3-air flames. They concluded that for NH_3-air mixtures at NTP, the radiation-induced uncertainty exceeds 15% when $\phi \leq 0.8$ or $\phi \geq 1.4$. Recently, Zheng et al. [39] used a Statistical Narrow-Band (SNB) model [40,41] in PREMIX code [38] to assess the effect of radiation reabsorption in steady freely propagating NH_3/H_2-air flame at different pressures and equivalence ratios. They found that, although the radiation effect predicted by OTM is very similar to adiabatic results, the maximum reabsorption effect reached 15.6% compared to the OTM model for NH_3/H_2-air flames. Zheng et al. [39] used freely propagating planar flames which has considerably larger optical thickness than the expanding spherical flames. Consequently, the predicted radiation reabsorption effect in [39] is much higher than the one in spherically propagating flames. Although these studies provide valuable insight on the importance of radiation in ammonia blends, they are not able to predict the radiation effect in LFS measured in SPF experiments. Further, the study of radiation in these flames is important to understand its impacts on emissions formation. Ilbas [42] denoted how radiation effects can decrease NO from 1000 to 200 ppm in H_2/CH_4 flames. Daguse et al. [43] found that NO mole fractions were underestimated by ~25% when radiation effects were not considered in $H_2/O_2/N_2$ diffusive flames. Therefore, it is essential to acknowledge the effect of the radiation on ammonia-based flames, not only to understand flame phenomena but also to accurately predict pollutant emissions when using this chemical.

To the best of the authors' knowledge, the radiation-induced uncertainty in spherically propagating NH_3-air, NH_3/CH_4-air, and NH_3/H_2-air flames has not been studied yet. Therefore, the aim of this study is to quantify the effects of radiation on spherically propagating NH_3-air, NH_3/CH_4-air, and NH_3/H_2-air flames at normal temperatures and pressures and different equivalent ratios and to provide quantitative assessment of the importance of radiation uncertainties and to investigate the possible approach to correct the measured LFS in SPF experiments.

This paper considers both 1D planar and 1D spherically propagating premixed flames. Two models, the adiabatic (ADI) model and the optical thin model (OTM), are used to analyze the effects of radiation. Specifically, planar flames are used to compare the ADI and OTM models for different mechanisms developed based on SPF, a jet-stirred reactor, and a tubular flow reactor, in order to assess the effects of radiation on these different mechanisms. Using the spherical flame, we explain how radiation affects the determination of laminar flame speed and assess for which mixtures radiation-induced uncertainty is significant. Finally, we demonstrate how the radiation effect can be corrected in SPF measurements. It should be noted that the radiation reabsorption effect is not investigated in this paper; however, we conducted simulations for spherically propagating NH_3-air, and NH_3/H_2-air flames using the SNB-CK model [30,40] and considering the radiation reabsorption of H_2O. The discrepancy between results from OTM and SNB-CK was found to be less than 2%.

2. Numerical methods

Both 1D steady planar and positively-stretched unsteady spherically propagating flame configurations are considered in this study. The PREMIX code [38] was used to simulate the planar steady flame and to get the flame structure and unstretched LFS. Thermal diffusion and multicomponent molecular transport models were included in all the simulations. To control gradient and curvature, the adaptive mesh parameters GRAD and CURVE were set to 0.01 in all simulations to obtain well resolved flame structures.

The in-house code ASURF [27,44,45] was used to simulate SPF [46,47]. The finite volume method was used in ASURF to solve the conservation equations for compressible, multicomponent, reactive flows, and the spherical coordination system was used in the formulations. The CHEMKIN package [48] which calculates the transport properties, thermodynamic properties and reaction rates was incorporated into ASURF. ASURF has been successfully used in previous studies to investigate the radiation effect [30-32,49] on SPF and alternative fuels [46,50,51]. The readers are referred to Refs. [44,52] for details on numerical schemes used in ASURF. To accurately resolve the spherical flame front, the dynamic adaptive mesh was used in the code. The finest mesh size of 16 μm and the smallest time step of 12 ns have been used in all the simulations. Numerical convergence of the simulations has been ensured by further decreasing the time step and mesh size and is provided as a supplementary material. To diminish the confinement effect [27,47], a large chamber radius of R_w=50 cm was used in all simulations.

In SPF, the unstretched laminar flame speed, $S_{b,0}$, and the Markstein length, L_b, both relative to the burned gas, are obtained from extrapolations using linear model, i.e., $S_b = S_{b,0} - L_b K$. The reason behind choosing the linear model over nonlinear model and the extrapolation range used in this paper is discussed in the next section. For a spherically propagating flame, stretch rate, K, is equal to $\frac{2}{R_f} \times \frac{dR_f}{dt}$ and $S_b = \frac{dR_f}{dt} - u_b$ where u_b is the flow speed of burned gas close to the reaction front. Usually only the flame front history R_f=$R_f(t)$ is recorded, as it is difficult to measure the flow speed of burned gas in experiments [53,54]. Consequently, the flame propagation speed is usually considered as the laminar flame speed relative to burned gas (i.e., $S_b \approx S$), and the accuracy of laminar flame speed measurement depends on the magnitude of the burned gas speed, i.e., $|u_b|$.

On the other hand, different factors affect the accuracy of LFS measurements in SPF as discussed in [18]. In this study, the authors focused on the influence of radiation, thereby other factors such as buoyancy and flame instability were not considered. To avoid the ignition effect in unsteady simulations, the flame is initiated using the extracted output temperature and mole fraction profiles for 1D planar premixed flames predicted by CHEMKIN-PREMIX.

The radiation effect was considered in simulations for both steady planar flames and SPF. The original PREMIX code was modified, and the optical thin model (OTM) was incorporated to take into account of the radiation effect. To validate this modified PREMIX code, the results obtained via PREMIX in Chemkin-Pro were compared with those calculated by Shindo and Nakamura [36] with the similar reaction mechanism for NH_3-air flames at T_u=298 K and $P = 1$ atm for $0.7 \leq \phi \leq 1.4$.

To include the radiation effect, the Planck-mean (PMAC) absorption coefficients were obtained from Hitran database [55] for

NH_3, H_2O, NO, N_2O, CH_4, CO, and CO_2. PMACs were used as a polynomial function of temperature to be compatible with the CHEMKIN thermodynamic format that is also incorporated in ASURF [27,40,56].

The detailed kinetics mechanisms were selected and used in all simulations of the steady planar flame and SPF. The mechanisms of Gotama et al. [8], Nakamura et al. [11], and Stagni et al. [57] were used to simulate the flame propagation in NH_3-air mixture. For simplicity, these mechanisms are named Gotama, Nakamura and Stagni in the following section. Gotama mechanism, which includes 32 species and 165 reactions, has been developed based on SPF measurements. Stagni mechanism, which includes 31 species and 203 reactions, was developed based on measurements performed using jet-stirred reactor and a tubular flow reactor. Finally, the Nakamura mechanism, which includes 38 species and 232 reactions, was developed based on data obtained from a micro flow reactor. The rationale of using these different mechanisms was to study the radiation effect in NH_3-air mixtures by comparing mechanisms that exhibit significant discrepancies in the measured LFS.

The concentration of ammonia in binary fuels NH_3/CH_4 and NH_3/H_2 is expressed in terms of ammonia heat fraction in the binary fuel [9];

$$E_{NH3} = \frac{X_{NH3} LHV_{NH3}}{X_{NH3} LHV_{NH3} + X_{\alpha} LHV_{\alpha}} \quad (1)$$

where X and LHV denote the mole fraction and lower heating value, and α is the second fuel used with ammonia, i.e., CH_4 or H_2.

The mechanism developed by Okafor et al. [9] was used for NH_3/CH_4-air mixtures. In this section the radiation effect for NH_3/CH_4-air mixtures at T_u=298 K and p = 1 atm and different equivalence ratios was studied. Similar to [9], three different E_{NH3} of 0.1, 0.2, and 0.3 are considered in this study.

Finally, for NH_3/H_2-air mixtures, the mechanism of Gotama et al. [8] was used. Here, we study the radiation effect for NH_3/H_2-air mixtures at T_u=298 K and p = 1 atm for 0.8≤ ϕ ≤1.8, when E_{NH3}=0.89 or equivalently the H_2 mole fraction in binary fuel, X_{H2}, equals 0.4.

It should be noted that we also used the Okafor mechanism [9] to study the radiation effect for the NH_3-air mixture. However, for rich NH_3-air mixture, the simulation results after including the radiation effect were not consistent with the ones from other mechanisms. Since the Gotama Mechanism [8] was developed based on the optimization of the Okafor Mechanism, and since it is more accurate than the Okafor Mechanism, the results obtained from the latter are not presented here.

3. Results and discussion

3.1. NH_3-air flames

The laminar flame speed measurements of NH_3-air mixtures in the literature at normal temperature and pressure [13-17,58,59] (see Table 1) are plotted in Fig. 1. Lower discrepancy is observed for stoichiometric mixtures, whilst greater scattering is observed for off-stoichiometric conditions. Even for stoichiometric mixtures, the scattering reaches 15%. It is interesting to note that the discrepancy at non-stoichiometric condition, i.e., ϕ=0.9 and 1.2, reaches 30%. This huge discrepancy in measured LFS directly influences the accuracy of the kinetic mechanisms of interest.

As mentioned earlier, the buoyancy and radiation effects are significantly important for NH_3-air as, $S_{u,0,}$ is less than 10 cm/s. The importance of buoyancy effect in SPF for mixtures with low LFS has already been discussed in [61]. The importance of the buoyancy effect can also be explained by observing Fig. 1, and comparing the results obtained by Ronney [13], in which the SPF experiments were done in micro-gravity condition. The reported LFS results by Ronney were considerably higher than the ones from other researchers with the exception of work by Mei et al. [17] which was not performed under micro-gravity conditions.

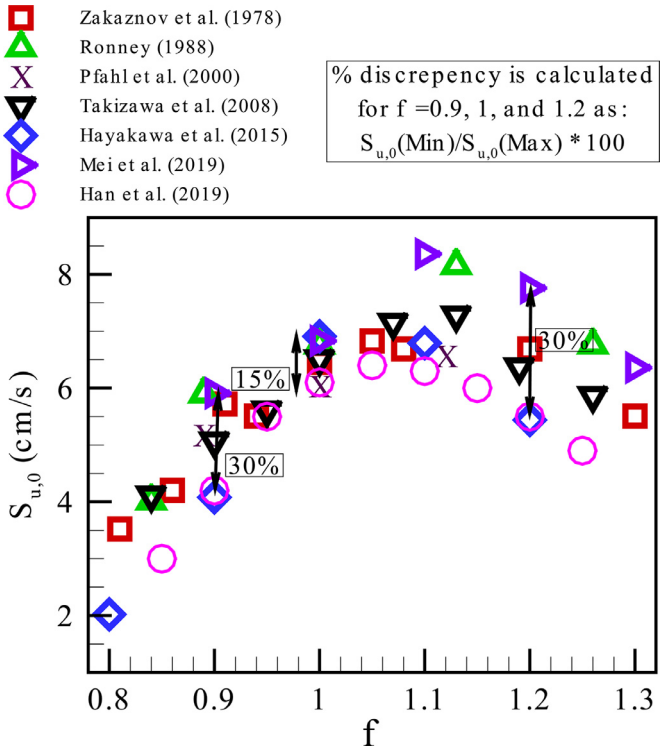

Fig. 1. Measured laminar flame speed for NH_3-air mixtures at normal temperature and pressure for 0.8≤ ϕ ≤1.3 obtained from the literature [13-17,58,59].

To isolate the radiation effect in this study we needed to choose the proper extrapolation method and flame radius ranges, which is discussed here. There are mainly three different extrapolation methods used in SPF to extract unstretched laminar flame speed [28]:

$$S_b = S_{b,0} - L_b K \quad (LM)$$

$$S_b = S_{b,0} - S_{b,0} L_b \frac{2}{R_f} \quad (NM1)$$

$$\ln(S_b) = \ln(S_{b,0}) - S_{b,0} L_b \frac{2}{R_f S_b} \quad (NM2)$$

As shown by Chen [62] and Wu et al. [28], depending on the Markstein length (L_b), it is expected that either LM, NM1, or NM2 would be more accurate to extract unstretched laminar flame speed,$S_{u,0}$. It was suggested in [62], to use NM2 for mixtures with negative L_b and NM1 for mixtures with large positive L_b. In this study, we compared the Markstein length for lean, stoichiometric, and rich mixtures to choose the proper extrapolation method. It was found that the unstretched laminar flame speed is highly sensitive to the extrapolation method and range for NH_3-air mixture. Figure 2 shows the normalized laminar flame speed for lean, stoichiometric and rich NH_3-air mixture as a function of the extrapolation range when 1 cm <R_f< 2 cm (i.e., $R_{f,L}$ = 1 cm) and 2 cm <R_f< 3 cm (i.e., $R_{f,L}$ = 2 cm). The laminar flame speeds determined either by NM1 or NM2 were normalized by LM. It was found that for lean mixture (Fig. 2a) when radiation is included the Markstein length is negative, and for rich mixture (Fig. 2c), the Markstein length is more than 3. Consequently, if we choose $R_{f,L}$ = 1 cm for the extrapolation range, it had been logical to use NM2 for

Table 1
Previous experimental studies on LFS measurement of NH_3-air mixtures at normal temperature and pressure.

Author(s), year	T_u (K)	P (atm)	ϕ	Method	$S_{u,0}$ at ϕ=1 (cm/s)	Notes*
Zakaznov, 1978, [14]	293	1	0.8–1.3	Cylindrical Flame Tube Method	6.3	d_i=5.4 cm; h = 130 cm
Ronney, 1988, [13]	Normal temperature**	1	0.85–1.25	Cylindrical chamber- constant pressure method	6.78	d_i=25 cm, h = 25 cm micro-gravity condition
Takizawa, 2008, [16]	Normal temperature**	1.05	0.9–1.2	Spherical chamber- constant pressure method	6.6	d_i=18 cm
Takizawa, 2008, [16]	Normal temperature**	1.05	0.9–1.2	Spherical chamber- constant volume method	6.75	d_i=18 cm
Hayakawa, 2015, [58]	298	0.987	0.7–1.3	Cylindrical chamber- constant pressure method	6.8	d_i=27 cm, h = 41 cm $\Delta S_{u,0}$**=0.7 (cm/s)
Mei, 2019, [17]	298	1	0.9–1.3	Cylindrical chamber- constant pressure method	6.53	d_i=15 cm, h = 15.2 cm $\Delta S_{u,0}$**=0.6 (cm/s)
Han, 2019, [59]	300	1	0.7–1.6	Heat flux method	6.15	$\Delta S_{u,0}$**=0.6 (cm/s)
Lhuillier, 2019, [60]	298	1	0.9–1.1	Spherical chamber- constant pressure method	6.45	6.15 cm/s< $S_{u,0}$<7.22 cm/s

* d_i and h denote the size of inner diameter and height of the chamber, respectively.
** $\Delta S_{u,0}$ is the reported uncertainty of the measurements.

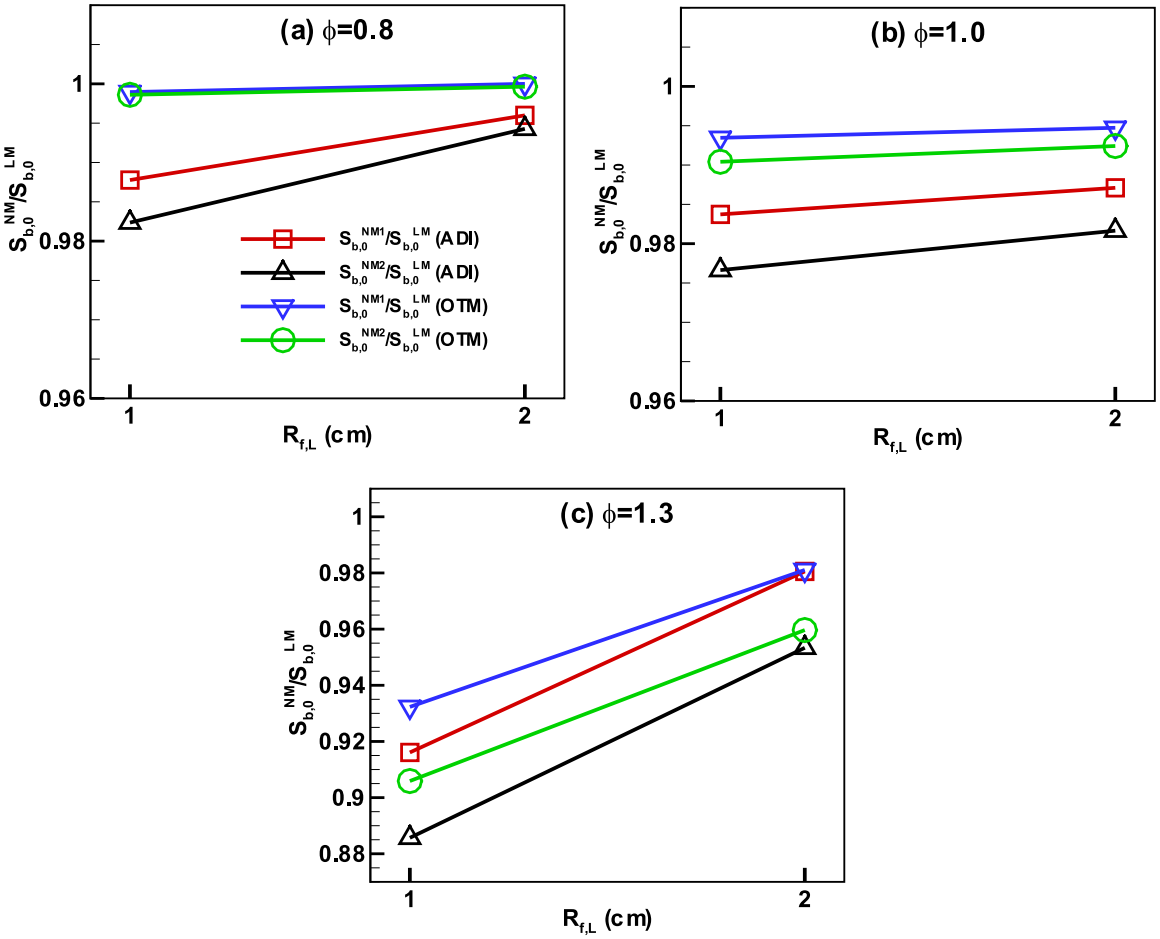

Fig. 2. Normalized laminar flame speed extrapolation based on different flame radius ranges of [$R_{f,L}$, $R_{f,L}$ + 1 cm] for NH_3-air flames at (a) φ= 0.8, (b) φ= 1.0, (c) φ= 1.3 and NTP.

lean mixtures and NM1 for rich mixtures. However, we intended to isolate the radiation effect in this study and avoid using different extrapolation methods for different equivalence ratios. It was found that by increasing the lower range of extrapolation, i.e., $R_{f,L}$, the discrepancy between LM, NM1, and NM2 would diminish. As shown in Fig. 2, the discrepancy between LM and NM2 is less than 1% and for rich mixture and that between LM and NM1 is within 2% for lean mixture. As a result, by choosing 2 cm <R_f< 3 cm we were able to acquire similar accuracy from LM, NM1 and NM2 and we were able to only use linear model to extract unstretched laminar flame speed. It is noted that due to the confinement effect and the amplification of radiation effect for $R_{f,L}$>2 cm, it is not a viable option to increase the extrapolation range beyond 2 cm <R_f< 3 cm.

To further justify the flame radius ranges to do the extrapolation, Fig. 3 shows the flame propagation speed with respect to the burned gas, S_b, as a function of stretch rate, K, for lean, stoichiometric, and rich NH_3-air mixtures at T_u=298 K and P = 1 atm. The dashed and solid lines in the figure show the linear extrapolation to zero stretch rate (based on LM), when 1 cm<R_f<2 cm and 2 cm<R_f<3 cm, respectively. The squares and circles represent the ADI simulation, and the diamonds and triangles represent the radiation included simulation using the OTM model. When ϕ=0.8 (Fig. 3a), the linear stretch formulation is accurate for both

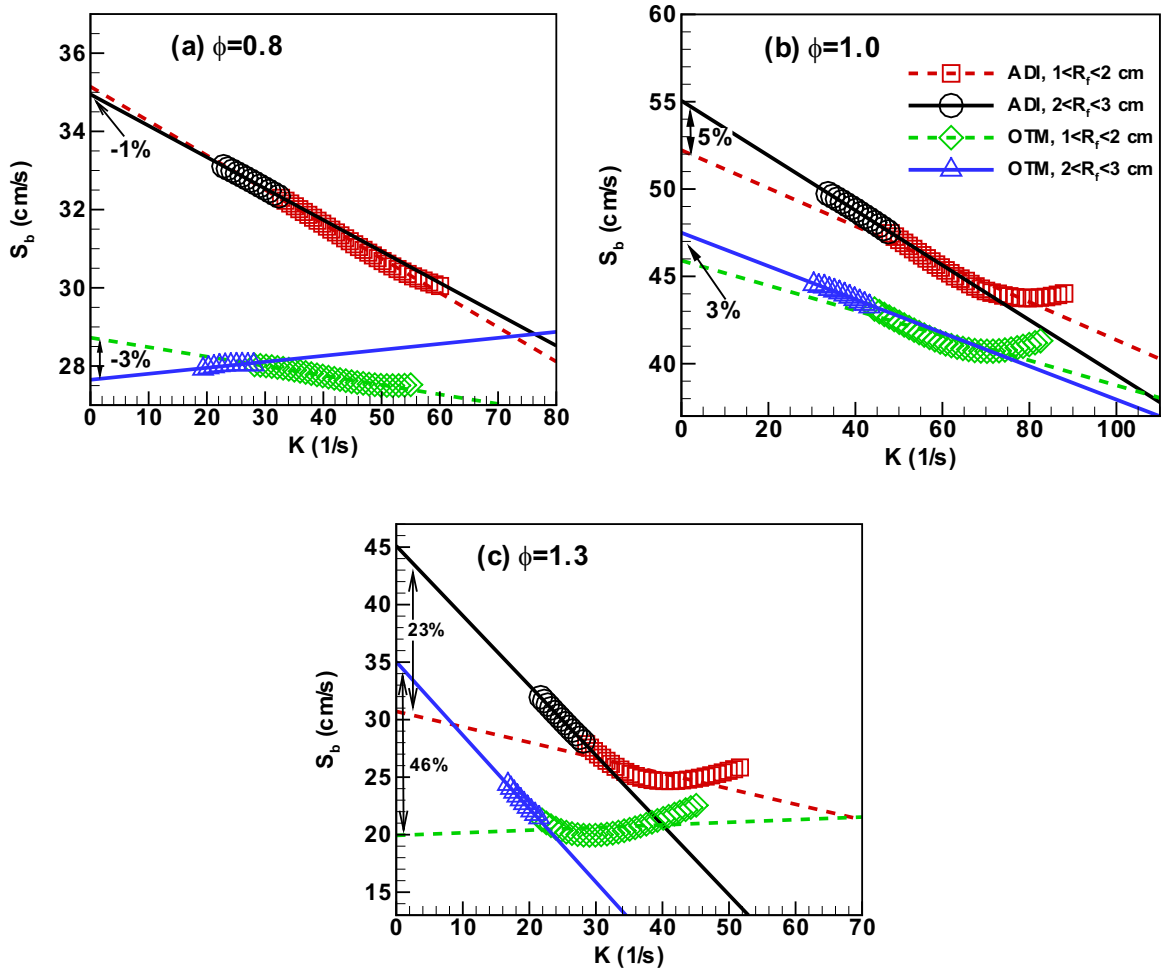

Fig. 3. Change of the flame speed relative to burned gas, S_b, with stretch rate, K, for spherical NH_3-air (ϕ=0.8, 1, and 1.3) flames at T_u=298 K and P = 1 atm. The symbols are data for spherical flames; the dashed and solid lines stand for linear extrapolation according to LM with 1 cm<R_f <2 cm and 2<R_f <3 cm, respectively. The discrepancy between unstretched laminar flame speed with respect to burned gas, $S_{b,0}$, between the extrapolated data for 1 cm<R_f <2 cm and 2 cm<R_f <3 cm is shown. Gotama mechanism is used in the simulations.

1 cm<R_f<2 cm and 2 cm<R_f<3 cm, and the range influence of the extrapolation on $S_{b,0}$ is less than 3%. Referring to Fig. 3b, the initiation effect of flame radius on extrapolation method becomes considerable for stoichiometric mixtures when 1 cm<R_f<2 cm; however, by increasing the extrapolation range to 2 cm<R_f<3 cm, S_b would change linearly with K, similar to what is shown in Fig. 2b. It is also noted that when ϕ=1.0, the deviation between $S_{b,0}$ defined by 1 cm<R_f<2 cm and 2 cm<R_f<3 cm reaches to 5%. Finally, for rich NH_3-air mixtures, e.g., ϕ=1.3 for 1 cm<R_f<2 cm, the extrapolation effect is significant, and it is necessary to use 2 cm<R_f<3 cm for linear extrapolation. The discrepancy between the $S_{b,0}$ based on 1 cm<R_f<2 cm and 2 cm<R_f<3 cm reaches 23% and 46% for ADI and OTM, respectively. The results presented in Figs. 2 and 3, indicate that when using 1 cm < R_f < 2 cm for stoichiometric and rich mixtures, the computation of $S_{b,0}$ led to under-prediction and inaccurate determination of the radiation effect. Based on the results obtained and to avoid initiation effect of flame radius on extrapolation method for radiation induced uncertainty investigations, LM for the flame radius ranging from 2 to 3 cm was used in all the simulations.

Since the negative burned gas velocity increases with the flame radius [31], it is anticipated that the radiation-induced uncertainty would increase with the flame radius. However, the under-prediction of $S_{b,0}$ in the current study when 1 cm<R_f<2 cm is due to the exceptionally low laminar flame speed of NH_3-air mixtures. Since the PREMIX results have been used in the current study to initiate the SPF, it takes time for the propagating spherical flame to reach the quasi-steady condition and the initiation effect to become negligible. Similar effects are also expected from SPF experiments for NH_3-air mixture with low LFS. However, unlike the current simulations, the inaccuracy of the extrapolation from low flame radii in experiment is expected to originate from the high ignition energy that is required for NH_3-air flame to initiate. Further investigation is needed to choose the proper extrapolation method and flame radii ranges for ammonia blends in SPF.

The performance of different mechanisms to predict, $S_{u,0}$, using steady planar flames (PREMIX code), with ADI and OTM models were studied in Fig. 4a. The solid lines represent the ADI calculations, and the dashed lines show the OTM results. While the Gotama mechanism predicts larger $S_{u,0}$ when $\phi \leq$1.1, Stagni mechanism predicts larger $S_{u,0}$ for $\phi \geq$1.2. The maximum discrepancy of the predicted $S_{u,0}$ based on Nakamura, Stagni and Gotama mechanisms for ϕ =0.7, 1 and 1.5 are 15%, 10% and 16%, respectively. The large deviation between the predicted $S_{u,0}$ by different mechanisms is related to the huge uncertainty in LFS measurement and different experimental methods that have been used as is shown in Fig. 1. The relative LFS, $S_{u,0}{}^{OTM}/S_{u,0}{}^{ADI}$, as a function of equivalence ratio for each mechanism is shown in Fig. 4b. It is noteworthy to see that the change of relative LFS based on Nakamura mechanism is the same as the one calculated earlier by Nakamura and Shindo [36]. Although the same PMAC has been used in all the simulations, the predicted relative LFS based on different mecha-

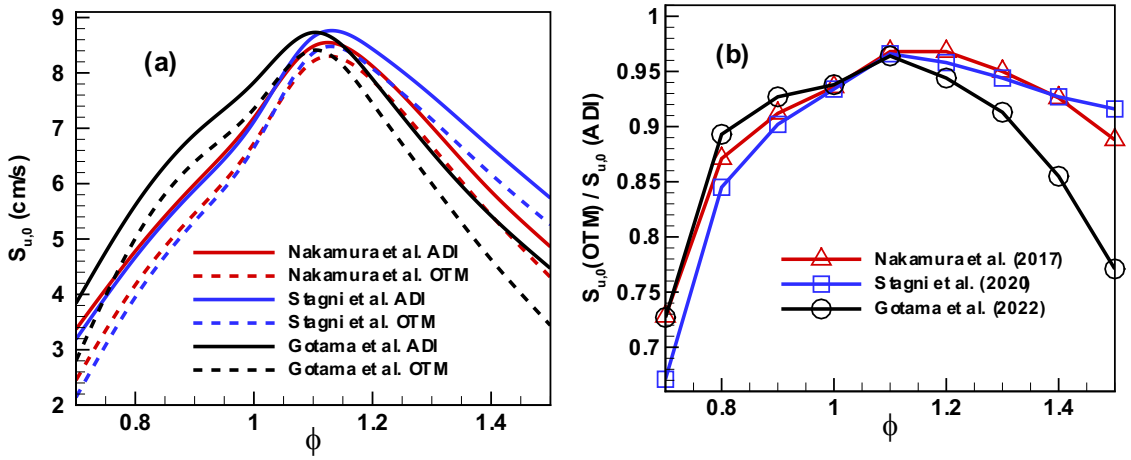

Fig. 4. (a) Computed adiabatic (solid lines) and radiative (dashed lines) flame speeds for freely propagating NH_3-air flames, and (b) the relative laminar flame speed with and without radiation heat loss. T_u=298 K and P = 1 atm. The Nakamura et al. [11], Stagni et al. [57] and Gotama et al. [8] mechanisms have been used in the calculations. The PREMIX code [38] has been used to calculate the laminar flame speed.

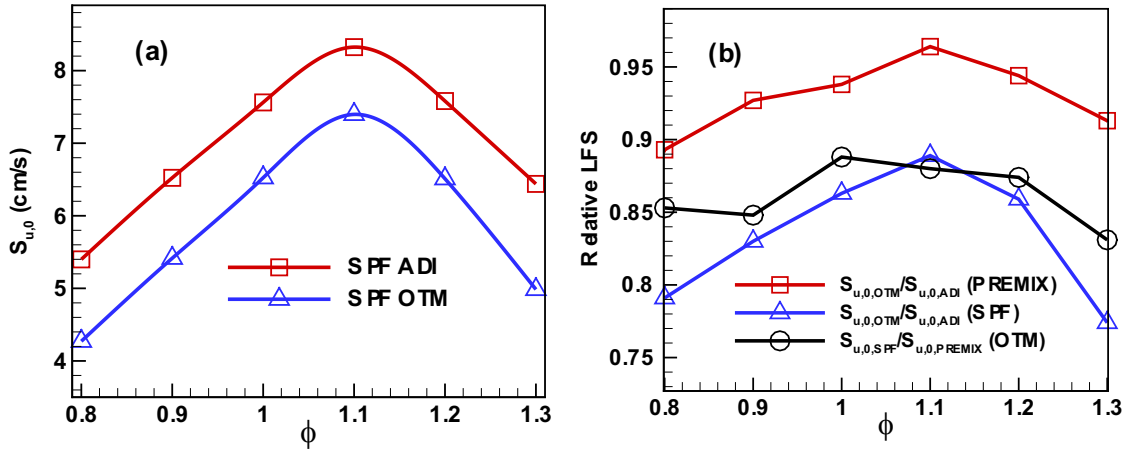

Fig. 5. (a) Laminar flame speed calculated using SPF with and without radiation, and (b) the normalized LFS for NH_3-air flames at T_u=298 K and P = 1 atm. Gotama mechanism is used in the simulations.

nisms scatter significantly for lean and rich mixtures. For ϕ =0.7, the relative LFS is less than 75% based on all mechanisms and it reaches 67% based on Stagni mechanism. Meanwhile, the relative LFS based on Stagni and Nakamura mechanism do not exceed 10% for rich mixtures but reaches up to 21% for ϕ =1.5, based on Gotama mechanism.

Apart from the differences in reaction coefficients that have been used in these different mechanisms, the importance of the radiation effects in the experimental methods to develop the former has also direct effects in the scattering between the relative laminar flame speeds. Since the focus of this study is to quantify the radiation-induced uncertainty in LFS determination using SPF measurements, and Gotama mechanism is the one obtained based on SPF experiments, we have used the Gotama mechanism to study the radiation effect in SPF for NH_3-air mixtures.

Figure 5a compares the $S_{u,0}$ calculated using ADI and OTM as a function of equivalence ratio. As anticipated, the radiation inclusion reduces the $S_{u,0}$ significantly. The mechanism of LFS reduction in SPF by radiation effects will be discussed further in Fig. 6. To compare the importance of the radiation in steady planar flame and SPF, Fig. 5b shows the relative LFS for planar steady flames, ${S_{u,0}}^{\circ TM}/\ {S_{u,0}}^{ADI}$ *(PREMIX)*, SPF, ${S_{u,0}}^{\circ TM}/\ {S_{u,0}}^{ADI}$ *(SPF)*, and the relative laminar flame speed including the radiation effect based on SPF and planar steady flames, ${S_{u,0}}^{SPF}/\ {S_{u,0}}^{PREMIX}$ *(OTM)*. Comparing ${S_{u,0}}^{\circ TM}/\ {S_{u,0}}^{ADI}$ *(PREMIX)* and ${S_{u,0}}^{\circ TM}/\ {S_{u,0}}^{ADI}$ *(SPF)*, the results show how the radiation-induced uncertainty increases in the studied spherically propagating flames. The black circles, which represent ${S_{u,0}}^{SPF}/\ {S_{u,0}}^{PREMIX}$ *(OTM)*, show that the radiation effect in SPF is around 15% greater than the one for planar steady flames, both including the radiation effect.

To further investigate the sources of radiation-induced uncertainties in SPF, the evolution of flow speed and temperature in a stoichiometric NH_3-air spherical flame were assessed, Fig. 6. A comparison between ADI and OTM shows the negative burned gas velocity after considering radiation heat loss. As was discussed earlier, conventionally the burned gas velocity is assumed to be zero, i.e., u_b = 0; while this assumption is true for adiabatic condition (solid lines in Fig. 6a), when the radiation is considered, inward flow in burned gas leads to u_b<0. Although this was already reported in previous works [34], the effect of negative burned gas velocity is much higher for NH_3-air spherical flames compared to conventional hydrocarbons and hydrogen blends in air. The importance of this negative burned gas velocity in NH_3-air is due to the low reaction rate of NH_3-air compared to CH_4-air and H_2-air. For H_2-air with LFS $\sim$ 200 cm/s at normal temperature and pressure, the same value of negative burned gas velocity induces much less uncertainty compared to NH_3-air with LFS as small as 5 cm/s. One way to avoid the uncertainty related to negative burned gas velocity is to use direct flow and flame front speed measurements with Particle Image Velocimetry (PIV) dur-

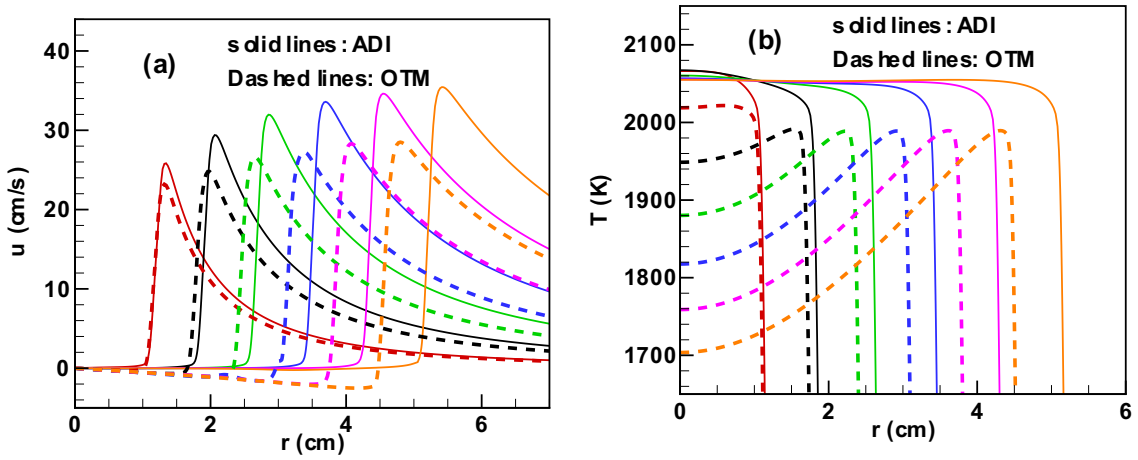

Fig. 6. Distributions of flow speed (a) and temperature (b) for propagating spherical stoichiometric NH_3-air at T_u=298 K and P = 1 atm. The distributions are at consecutive equidistant instants of time: t = 10, 30, 50, 70, 90 and 110 ms. Gotama mechanism is used in the simulations.

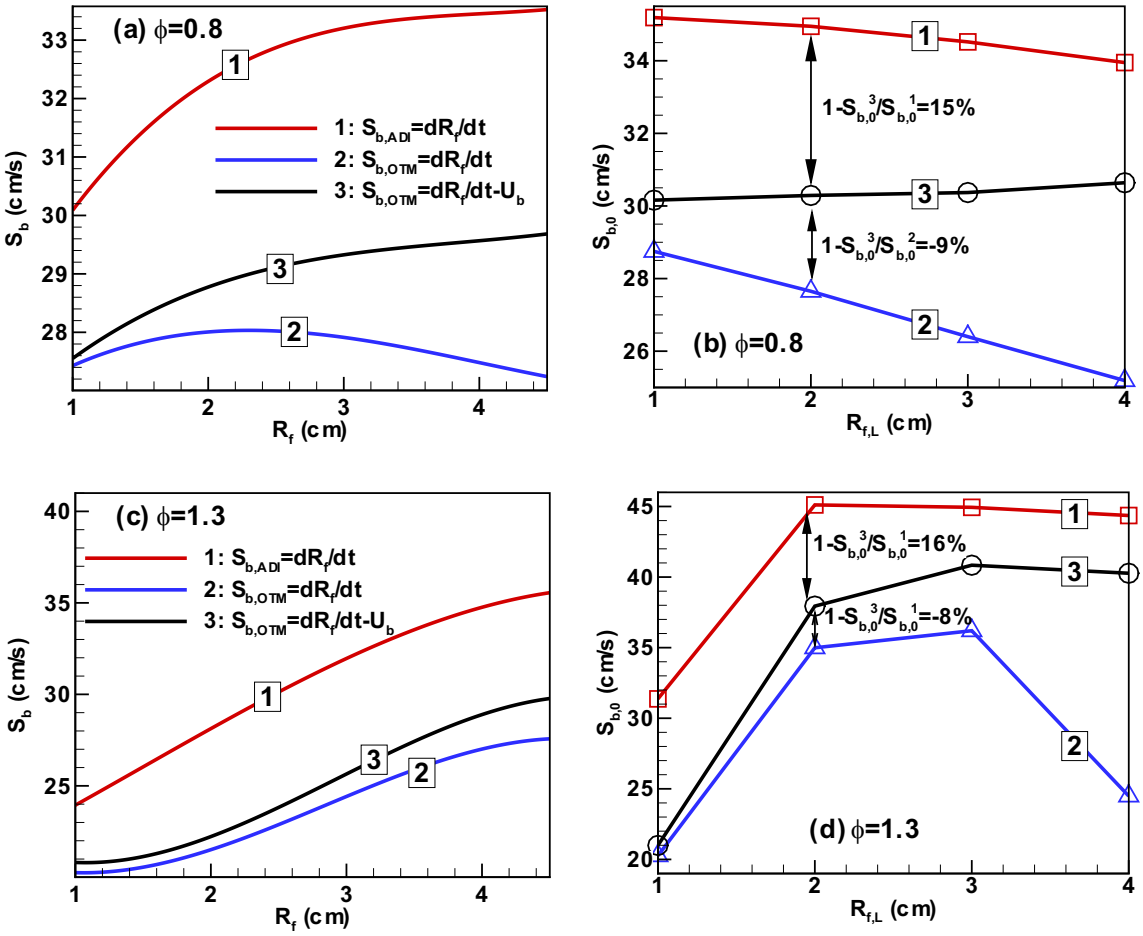

Fig. 7. Change of the flame speed relative to burned gas, S_b with flame radius (a & c), and unstretched flame speed relative to the burned gas with different flame radius ranges of [$R_{f,L}$, $R_{f,L}$ + 1 cm] (b & d) for lean and rich conditions using NH_3-air flames at T_u=298 K and P = 1 atm. Gotama mechanism is used in the simulations.

ing experiments [53]. Although this method has been used for hydrocarbon-air blends [63] and H_2-air [64], direct measurements have not been used for spherical NH_3-air flames. Figure 6b shows that the peak flame temperature is reduced after considering radiative loss. Due to radiation, the peak flame temperature constantly reduces in time and decreases by 250 K at t = 90 ms. Due to radiation-induced reductions in the flame temperature, the overall reaction rate decreases and so does the flame propagation speed. The flow velocity and temperature evolution in Fig. 6 also confirm that the radiation effect magnifies by flame propagation as negative burned gas velocity increases and the overall reaction rate decreases.

To differentiate between the radiation-induced flow and thermal effects that were observed in Fig. 6, Fig. 7(a & c) compares the stretched flame speeds relative to the burned gas by ADI and OTM under lean and rich conditions, i.e., ϕ =0.8 and 1.3. While

line 1 and 2 show dR_f/dt with and without radiation, line 3 shows the accurate $S_b(radiative) = \frac{dR_f}{dt} - u_b$. As a result, the difference between line 1 and line 3 is caused by radiation-induced thermal effect and the difference between line 2 and line 3 is caused by radiation-induced thermal effect. It was already shown in Fig. 6a, as flame propagates, that the magnitude of inward burned gas velocity increases and so does the difference between line 2 and line 3. This indicates that flow effects increase with the flame radius. As was discussed in [34], the inward flow is induced by radiation cooling due to mass conservation inside the spherical flame. Radiation cooling induces negative flow speed by decreasing the burned gas temperature and increasing its density. Comparing Line 1 and 3 shows that the radiation-induced thermal effect is less sensitive to flame size. To further investigate the effect of radiation-induced flow and thermal effect on unstretched laminar flame speed determination, Fig. 7(b & d) plot $S_{b,0}$ with flame radius ranges for ϕ = 0.8 and 1.3. flame radius ranges, $R_{f,L}$, in Fig. 7(b & d) are defined as [$R_{f,L}$, $R_{f,L}$ + 1 cm]. For ϕ = 0.8 (see Fig. 7b), line 2, for which U_b is assumed to be zero, diverges from line 3, for which the radiation-induced flow effect is considered. However for ϕ = 1.3 (see Fig. 7d), line 3 does not start to decrease at the various extrapolation ranges before $R_{f,L}$ = 3 cm. This can be justified with the results obtained in Fig. 3c and is originated from two different factors; firstly, as was shown in Fig. 3c, LM, that was used to determine $S_{b,0}$ is not accurate for rich NH_3-air mixture when 1 cm<R_f<2 cm and alternative extrapolation method may be more accurate [28]; and secondly, this can be attributed to the fact that when ϕ =1.3, the spherical flame does not reach quasi-steady propagation before R_f=2 cm and is still affected by initiation effect of flame radius on extrapolation method when 1 cm<R_f<2 cm. It is noted that in this study the ignition effect [18] is avoided by using the temperature profile obtained from PREMIX code to initiate the unsteady simulation. Further studies are needed to investigate the ignition effect on spherical flame propagation and to determine the appropriate extrapolation range that accounts for this effect. Finally, comparing Fig. 7c and Fig. 7d shows that the radiation-induced flow and thermal effect have similar influence for both lean and rich mixtures when $R_{f,L}$ = 2 cm. Meanwhile, the radiation-induced thermal effect is responsible for around 15% heat-loss, i.e., $S_{b,0}$ reduction, and the radiation-induced flow causes further 9% reduction of $S_{b,0}$.

3.2. NH_3/CH_4-air flames

Starting from a planar steady solution, the solid lines in Fig. 8 show the relative LFS, ${S_{u,0}}^{\circ TM}/{S_{u,0}}^{ADI}$, as a function of equivalence ratio for different E_{NH3}, calculated by PREMIX code. Based on Fig. 8, the calculated ${S_{u,0}}^{\circ TM}/{S_{u,0}}^{ADI}$ is always above 0.98 and decreases slightly by increasing the ammonia content. The dashed lines denote the ${S_{u,0}}^{\circ TM}/{S_{u,0}}^{ADI}$ based on SPF simulations. To keep the consistency with the procedures used for NH_3-air spherical flames, LM has been used to determine $S_{u,0}$ with the extrapolation range of 2 cm<R_f<3 cm. It is observed that the radiation-induced uncertainty has considerably increased for spherical flames compared to steady planar flames with the same E_{NH3}. Unlike steady planar flames, by increasing the ammonia content the radiation-induced uncertainty increases significantly for the same equivalence ratio; meanwhile for rich NH_3/CH_4-air spherical flames, ${S_{u,0}}^{\circ TM}/{S_{u,0}}^{ADI}$ is 0.96 for E_{NH3}=0.1, until it reaches 0.92 for E_{NH3}=0.3.

For the spherical flames, the reduction in ${S_{u,0}}^{\circ TM}/{S_{u,0}}^{ADI}$ produced by increasing E_{NH3}, Fig. 8, is related to the reduction of reaction rate of the mixture. Figure 9a shows that increasing E_{NH3} from 0.1 to 0.3, decreases LFS from around 25 cm/s to 15 cm/s for stoichiometric values. This in turn increases radiation heat loss by increasing radiation-induced flow and thermal effects, as discussed for NH_3-air mixtures in the previous section. Figure 9b shows ${S_{u,0}}^{SPF}/{S_{u,0}}^{PREMIX}$ *(OTM)* for E_{NH3}=0.1, 0.2 and 0.3. It is interesting to note that ${S_{u,0}}^{SPF}/{S_{u,0}}^{PREMIX}$(OTM) is relatively constant regardless of the equivalence ratio and decreases slightly by increasing E_{NH3}. This is in consistent with what was observed for ${S_{u,0}}^{SPF}/{S_{u,0}}^{PREMIX}$(OTM) behavior for NH_3-air mixtures in Fig. 5b at different equivalence ratios. This also shows that the relative relation between LFS defined by SPF and PREMIX when including radiation effect is relatively independent of equivalence ratio.

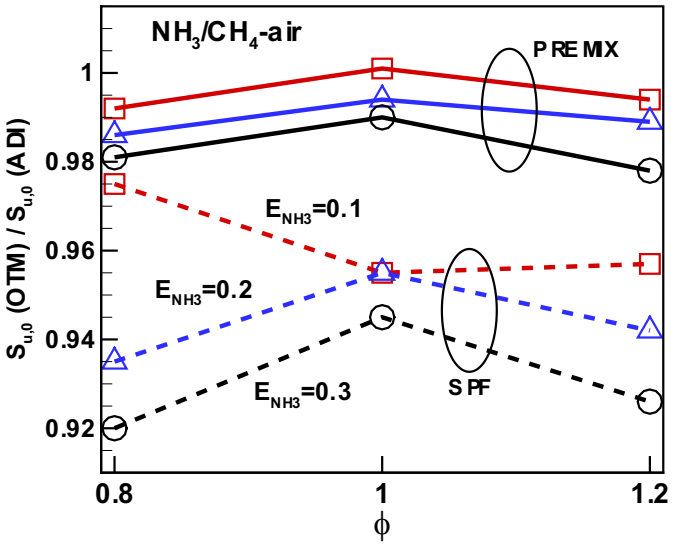

Fig. 8. Relative laminar flame speed (OTM to ADI) for freely propagating flames (solid lines) and SPF (dashed lines) as a function of equivalence ratio for NH_3/CH_4-air at T_u=298 K and P = 1 atm with different E_{NH3}. The red square, blue triangle, and black circle denote E_{NH3}=0.1, 0.2, and 0.3, respectively. The mechanism developed by Okafor et al. [9] was used. (For interpretation of the references to colour in this figure legend, the reader is referred to the web version of this article.)

3.3. NH_3/H_2-air flames

Figure 10a shows the LFS employing spherical flames using ADI and OTM for different equivalence ratios initially at T_u=298 K and P = 1 atm. Unlike NH_3-air, radiation heat loss only has minor effects on LFS. This is related to the higher LFS of NH_3/H_2-air compared to NH_3-air. To quantify the radiation induced uncertainty in SPF and compare it with steady planar calculations, Fig. 10b shows ${S_{u,0}}^{\circ TM}/{S_{u,0}}^{ADI}$ for planar steady flames (red line with squares) and SPF (blue line with triangle). ${S_{u,0}}^{\circ TM}/{S_{u,0}}^{ADI}$ for steady planar flame is identical to what was found in [39]. Similar to the radiation effect for NH_3-air and of NH_3/CH_4-air discussed in previous sections, the radiation induced uncertainty increases in spherically propagating flames and it reaches a maximum 6% for NH_3/H_2-air when ϕ =1.8. Remembering that radiation reabsorption can enhance the LFS for this mixture in planar steady flames [39], it can be expected that using the SNB model to include radiation reabsorption can compensate the radiation heat loss in spherical NH_3/H_2-air flames. However, Zheng et al. [39] used freely propagating planar flames which has considerably larger optical thickness than the expanding spherical flames. Consequently, the predicted radiation reabsorption effect in [39] is much higher than the one in spherically propagating flames. Further studies on the effect of radiation reabsorption in SPF to accurately quantify the uncertainty requires a separate study.

3.4. Radiation-corrected flame speed

It was observed that the radiation induced uncertainty in spherical ammonia-blend flames is considerable and needed to be cor-

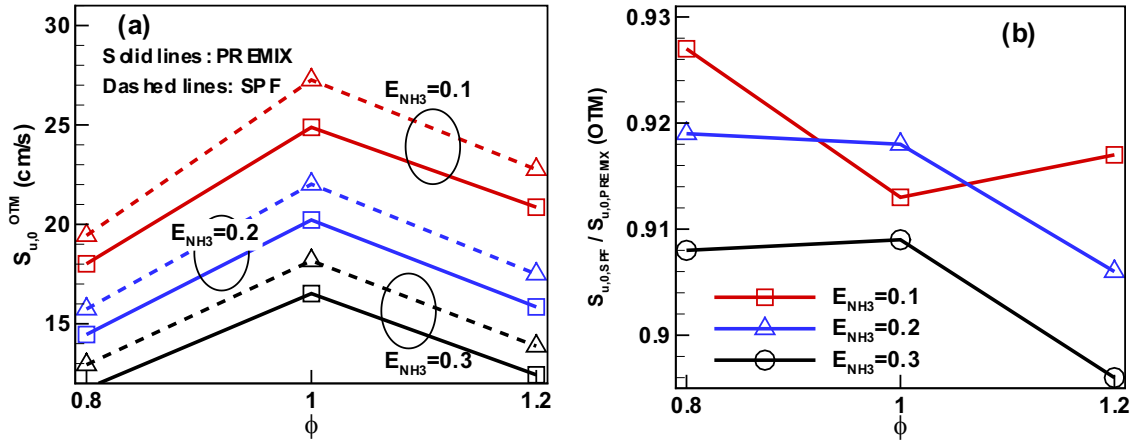

Fig. 9. (a) Laminar flame speed determined using PREMIX and SPF with radiation, and (b) the relative laminar flame speed, $S_{u,0}{}^{SPF}/\ S_{u,0}{}^{PREMIX}$ *(OTM)*, for NH_3/CH_4-air flames at T_u=298 K and P = 1 atm with different E_{NH3}. The mechanism developed by Okafor et al. [9] was used.

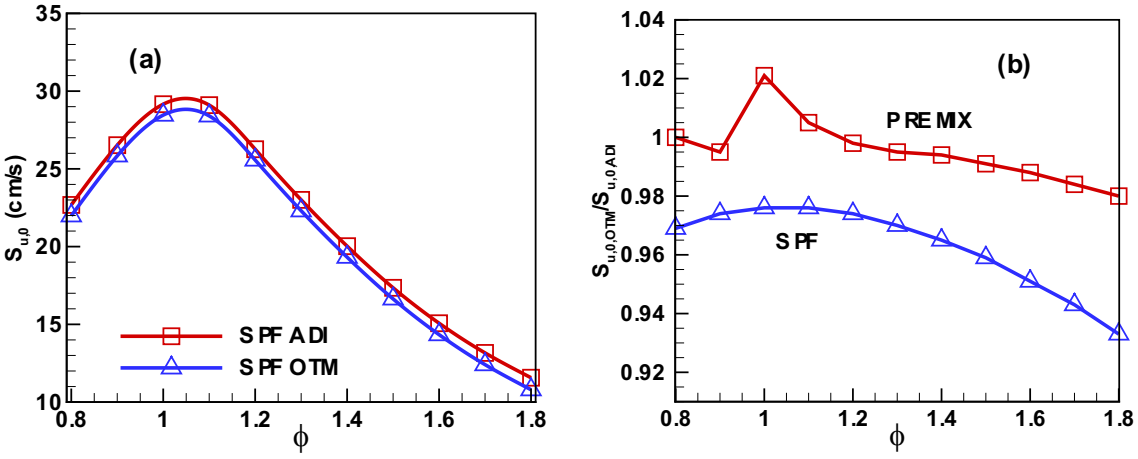

Fig. 10. (a) Laminar flame speed determined using SPF with and without radiation, and (b) relative laminar flame speed (OTM to ADI) for freely propagating flames (red square symbols) and SPF (blue triangle symbols) as a function of equivalence ratio for NH_3/H_2-air at T_u=298 K, P = 1 atm, and E_{NH3}=0.89. The mechanism developed by Gotama et al. [8] was used. (For interpretation of the references to colour in this figure legend, the reader is referred to the web version of this article.)

rected. Yu et al. [34] studied the radiation-induced uncertainty in different mixtures including hydrocarbons and H_2/CO blends in air using SPF simulations and the SNB model, and introduced a single correlation to correct the radiation induced uncertainty in experiments for different fuel-air mixtures with a variety of equivalence ratios, initial temperatures and pressures. Defining the relative reduction in unstretched laminar flame speed caused by radiation, R, as

$$R = 1 - \frac{S_{b,0}^{radiative}}{S_{b,0}^{ADI}} \tag{2}$$

where $S_{b,0}$ is the unstretched laminar flame speed with respect to burned gas, with the unstretched laminar flame speed with respect to the unburned gas being $S_{u,0}$, which is commonly approximated as $S_{u,0} \approx (\rho_b/\rho_u)_{eq}\ S_{b,0}$. In this equation, $(\rho_b/\rho_u)_{eq}$ denotes the density ratio in equilibrium conditions. This simple approximation, also used in this study, avoids the complexity of defining the accurate density ratio for different conditions that were considered in [46,51]. Using $(\rho_b/\rho_u)_{eq}$ Yu et al. [34] defined the correlation at normal temperatures and pressures;

$$S_{u,0}^{ADI} - S_{u,0}^{radiative} = 0.82 S_{u,0}^{ADI} \left(\frac{S_{u,0}^{ADI}}{S_0} \right)^{-1.14} \tag{3}$$

S_0 in the above equation is equal to 1 cm/s.

Figure 11a shows R versus the adiabatic laminar flame speed, $S_{u,0}{}^{ADI}$. The solid line shows the R prediction based on Eq. (3) and symbols denote the accurate R for NH_3-air, NH_3/CH_4-air, and NH_3/H_2-air initially at T_u=298 K and P = 1 atm. It is observed that Eq. (3) predicts the trend of R reduction with $S_{u,0}{}^{ADI}$ accurately. Furthermore, looking at Fig. 11b that plots the "%Error" of Eq. (3) compared to accurate R values directly computed using Eq. (2), the accuracy of the correlation for NH_3/CH_4-air and NH_3/H_2-air is confirmed; it is observed that "%Error" does not exceed 4% for these mixtures. It should be noted that Yu et al. [34] determined $S_{u,0}{}^{radiative}$ considering the radiation reabsorption for CO_2, CH_4 and H_2O. However, here we only considered the radiation heat loss using OTM, and radiation reabsorption is not considered. It is expected that considering the radiation reabsorption in simulations may improve the accuracy of the correlation even further for NH_3/CH_4-air and NH_3/H_2-air. However, looking at Fig. 11 shows that the correlation is unable to predict R accurately for NH_3-air and "%Error" increases by reducing $S_{u,0}{}^{ADI}$ as it reaches 15% for $S_{u,0}{}^{ADI}$=5 cm/s. Since the correlation works well for both NH_3/CH_4-air and NH_3/H_2-air, it can be stated that the main conclusion made by Yu et al. [34] around the relation between R and LFS, which shows nearly independency between the fuel type and equivalence ratio, is valid. It is important to notice that the mixtures used in [34] to adopt the correlation have laminar flame speeds above 9 cm/s and the error in R predicted by Eq. (3) for

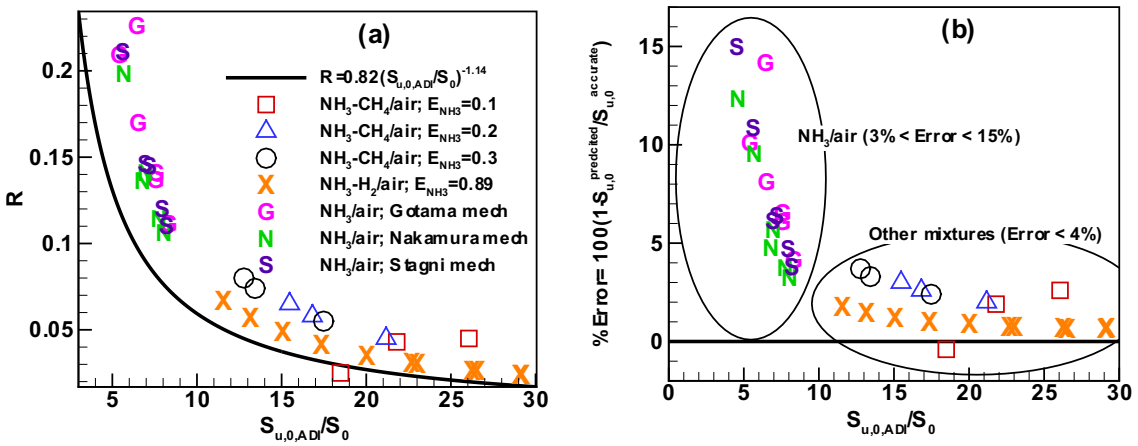

Fig. 11. Relative laminar flame speed reduction, R, (a) and the correlation error (b) as a function of normalized laminar flame speed, $S_{u,0,ADI}/S_0$ (where S_0=1 cm/s), for NH_3-air, NH_3/CH_4-air, and NH_3/H_2-air. Okafor and Gotama mechanisms have been used for NH_3/CH_4-air, and NH_3/H_2-air mixtures, respectively. The mechanisms used to simulate SPF for NH_3-air are stated in the figure. T_u=298 K and P = 1 atm. The solid line in (a) is the correlation developed in [34].

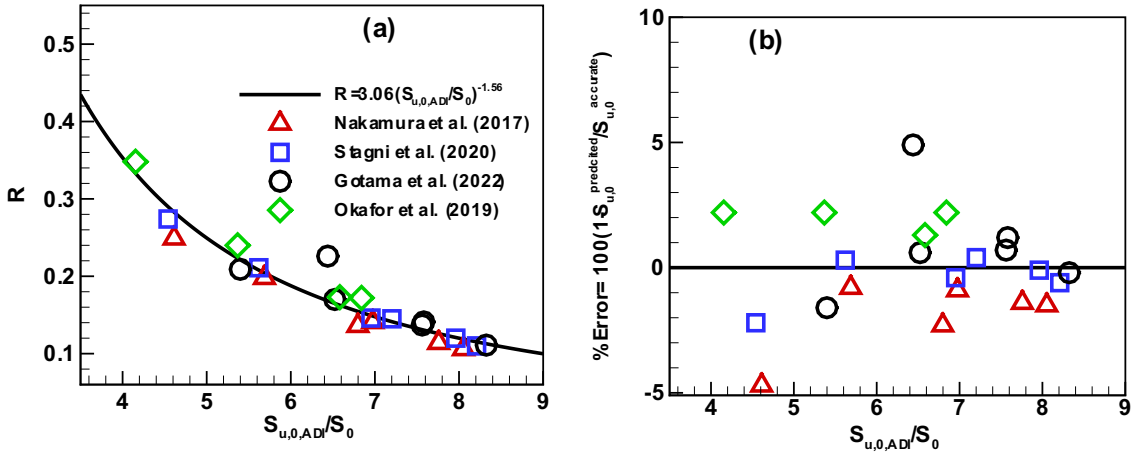

Fig. 12. Relative laminar flame speed reduction, R, (a) and the correlation error (b) as a function of normalized laminar flame speed, $S_{u,0,ADI}/S_0$ (where S_0=1 cm/s), for NH_3-air using Nakamura, Stagni, Gotama, and Okafor mechanism. T_u=298 K and P = 1 atm. The solid line in (a) is the correlation newly correlation developed here, Eq. (4).

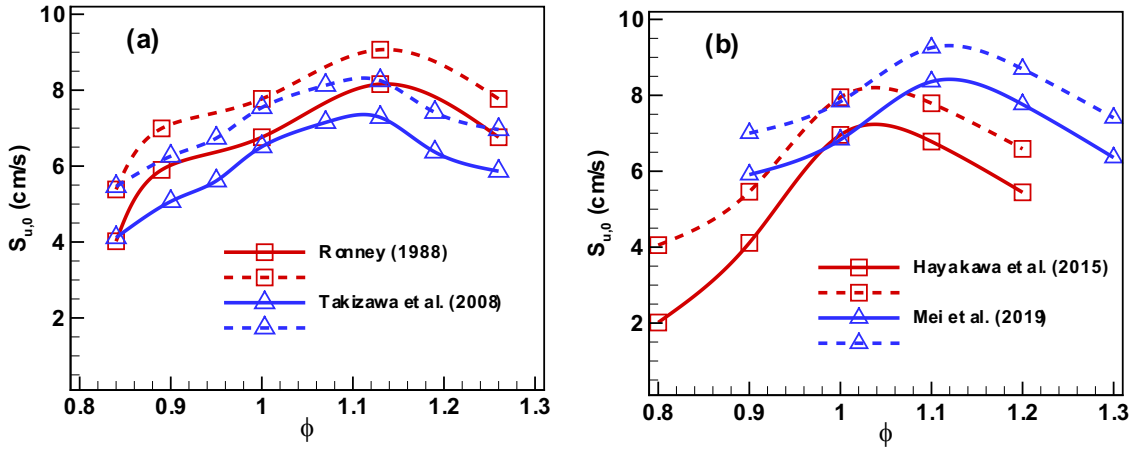

Fig. 13. Measured laminar flame speed using SPF experiments for NH_3-air mixtures at normal temperature and pressure for $0.8 \leq \phi \leq 1.3$ based on (a) Ronney [13] and Takizawa et al. [16], and (b) Hayakawa et al. [58] and Mei et al. [17].. The solid lines denote radiation included LFS, $S_{u,0}^{EXP}$, and dashed lines denote the radiation corrected ones, $S_{u,0}^{RC}$, using Eq. (5).

NH_3-air mixtures can be associated to the fact that LFS for this mixture is always less than 8 cm/s.

To further extend the application of Eq. (3), the LFS calculated with and without radiation heat-loss for NH_3-air using Okafor, Gotama, Nakamura and Stagni mechanism have been used to develop a correlation specifically for NH_3-air with $S_{u,0}$<9 cm/s;

$$\text{For } S_{u,0} < 9 \text{ cm/s}: S_{u,0}^{ADI} - S_{u,0}^{radiative} = 3.06 S_{u,0}^{ADI} \left(\frac{S_{u,0}^{ADI}}{S_0} \right)^{-1.58} \quad (4)$$

The LFS determined by Okafor mechanism for NH_3-air spherical flames for ϕ =1.2 and 1.3 are not used to develop Eq. (4). This is because the Okafor mechanism underpredicts $S_{u,0}{}^{\text{radiative}}$ by more than 35% and 65% for ϕ =1.2 and 1.3 when compared to other mechanisms. Figure 12a compares the relative laminar flame speed reduction predicted by Eq. (4) and the accurate definition of Eq. (2). It is observed that Eq. (4) is able to predict R accurately for spherical NH_3-air flames initially at T_u=298 K and P = 1 atm and different equivalence ratios. To further calculate the uncertainty of using Eq. (4) to predict $S_{u,0}$, Fig. 12b shows the correlation error as a function of normalized flame speed. It can be observed that the scattering between the accurate $S_{u,0}$ and the one predicted by Eq. (4) is less than 5% for all the mechanisms disregarding equivalence ratio. Remembering radiation induced uncertainty for lean and rich spherical NH_3-air flames reaches up to 25% (Fig. 5b), the updated correlation can significantly improve the accuracy of LFS measurements in SPF for NH_3-air flames.

The laminar flame speed measured in SPF experiments, $S_{u,0}{}^{\text{EXP}}$, is close to the radiative one, i.e., $S_{u,0}{}^{\text{EXP}} \approx S_{u,0}{}^{\text{radiative}}$ and the radiation corrected LFS is equal to $S_{u,0}{}^{\text{ADI}}$, $S_{u,0}{}^{\text{RC}} = S_{u,0}{}^{\text{ADI}}$. Combining Eqs. (3) and (4) and using the Newton iteration method, once the laminar flame speed is measured by SPF experiments, the radiation corrected LFS can be estimated as;

$$\begin{cases} \text{For } S_{u,0}^{EXP} \le 9 \text{ cm/s}: S_{u,0}^{RC} = S_{u,0}^{EXP} + 3.06 S_{u,0}^{EXP} \left(\frac{S_{u,0}^{EXP}}{S_0} \right)^{-1.58} \\ \text{For } S_{u,0}^{EXP} > 9 \text{ cm/s}: S_{u,0}^{RC} = S_{u,0}^{EXP} + 0.82 S_{u,0}^{EXP} \left(\frac{S_{u,0}^{EXP}}{S_0} \right)^{-1.14} \end{cases} \quad (5)$$

$S_{u,0}{}^{\text{RC}}$ can be further used in experiments instead of $S_{u,0}{}^{\text{EXP}}$, to develop and optimize the reaction mechanisms using spherically propagating flame experiments. Figure 13 plots the LFS measured using SPF experiments reported in [13,16,17,58]. The solid lines denote the measured LFS reported in the articles and the dashed lines are the radiation-corrected LFS determined in this study using Eq. (5). It is observed that the corrected laminar flame speeds increased significantly compared to the original LFS and these radiation-corrected LFS can furtherly be used to develop and optimize the detailed mechanisms for ammonia mixtures.

4. Conclusions

Numerical simulations with detailed chemistry and transport were conducted for planar and spherically propagating NH_3-air, NH_3/CH_4-air and NH_3/H_2-air flames with different equivalence ratios at normal temperature and pressure. The radiation effect was included in the simulations using the optical thin model, and the Planck-mean (PMAC) absorption coefficients were obtained from the Hitran database. The main findings were as follows:

1. The uncertainty in SPF was attributed to the radiation-induced flow and thermal effects. While the radiation-induced flow effect increases with flame radius, the thermal effect was relatively constant. The deviation between the LFS defined by planar and spherically propagating flames ($S_{u,0}{}^{SPF}/S_{u,0}{}^{PREMIX}$) was relatively constant disregard to the blend richness for all the mixtures. For NH_3-air flames it was around 15%. For NH_3/CH_4-air flames the deviation increased with ammonia content and reached up to 10% when E_{NH3}=0.3. Finally, for NH_3/H_2-air flames with E_{NH3}=0.89, the deviation decreased to around 4%.
2. For stoichiometric and rich NH_3-air flames, the initiation effect of flame radius on extrapolation method was considerable for 1 cm<R_f<2 cm; to avoid employing different extrapolation methods for different mixtures and conditions, the flame radii to do the extrapolation was set to 2 cm<R_f<3 cm. It was also shown that even the nonlinear model is unable to accurately predict the unstretched laminar flame speed for rich NH_3-air flames when 1 cm<R_f<2 cm. Although a qualitative match was found among the LFS using different mechanisms, they vary quantitatively; this was attributed to the fact that the radiation-induced uncertainty was not accounted for, changing on the basis of the experimental method.
3. For NH_3/CH_4-air flames, when ammonia content was increased, the radiation-induced uncertainty also increased, phenomenon that can be attributed to the longer residual time of the flame in the combustion chamber. NH_3/H_2-air flames were less affected by the radiation-induced uncertainty than other mixtures studied in this work.
4. It was shown that the correlation from [34] works well for NH_3/CH_4-air and NH_3/H_2-air flames, where the LFS is above 9 cm/s. However, this correlation is unable to predict the radiation-induced reduction for NH_3-air flames where LFS is less than 9 cm/s, and therefore a new correlation is proposed for NH_3-air flames. The newly developed correlation was further used to determine the radiation-corrected LFS in NH_3-air flames measured by SPF experiments and reported in [13,16,17,58]. The updated correlation, Eq. (5), can be used for different ranges of flame speeds regardless of the type of mixture.

It should be emphasised that Eq. (4) was only validated for NH_3-air, NH_3/CH_4-air, and NH_3/H_2-air flames. Further verification needs to be carried out to expand its application to other mixtures with low laminar flame speed, i.e., $S_{u,0}$< 9 cm/s. Hydrofluorocarbons with low LFS should be considered in future studies; however, based on [34], it is anticipated that changing the fuel type will not considerably affect the accuracy of Eq. (4). To further increase the accuracy of predicting radiation-induced uncertainty in ammonia blends in SPF experiments, future work should include the consideration of radiation reabsorption.

Declaration of Competing Interest

The authors declare that they have no known competing financial interests or personal relationships that could have appeared to influence the work reported in this paper.

Acknowledgments

We gratefully acknowledge financial support by the Engineering and Physical Science Research Council (EPSRC) through the grant number EP/T033800/1.

References

[1] A. Valera-Medina, et al., Ammonia for power, Prog. Energy Combust. Sci. 69 (2018) 63–102.
[2] C. Mounaïm-Rousselle, et al., Ammonia as fuel for transportation to mitigate zero carbon impact, engines and fuels for future transport, Springer, pp. 257–279.
[3] F.R. Westlye, et al., Experimental investigation of nitrogen based emissions from an ammonia fueled SI-engine, Fuel 111 (2013) 239–247.
[4] O. Kurata, et al., Development of a wide range-operable, rich-lean low-NOx combustor for NH_3 fuel gas-turbine power generation, Proc. Combust. Inst. 37 (2019) 4587–4595.
[5] O. Kurata, et al., Performances and emission characteristics of NH_3–air and NH_3CH_4–air combustion gas-turbine power generations, Proc. Combust. Inst. 36 (2017) 3351–3359.

[6] S. Ito, et al., Development of ammonia gas turbine co-generation technology, IHI Eng. Rev. 53 (2020) 1–6.
[7] A. Ichikawa, et al., Laminar burning velocity and Markstein length of ammonia/hydrogen/air premixed flames at elevated pressures, Int. J. Hydrogen Energy 40 (2015) 9570–9578.
[8] G.J. Gotama, et al., Measurement of the laminar burning velocity and kinetics study of the importance of the hydrogen recovery mechanism of ammonia/hydrogen/air premixed flames, Combust. Flame 236 (2022) 111753.
[9] E.C. Okafor, et al., Measurement and modelling of the laminar burning velocity of methane-ammonia-air flames at high pressures using a reduced reaction mechanism, Combust. Flame 204 (2019) 162–175.
[10] E.C. Okafor, et al., Experimental and numerical study of the laminar burning velocity of CH_4–NH_3–air premixed flames, Combust. Flame 187 (2018) 185–198.
[11] H. Nakamura, et al., Kinetic modeling of ammonia/air weak flames in a micro flow reactor with a controlled temperature profile, Combust. Flame 185 (2017) 16–27.
[12] C. Xiouris, et al., Laminar flame speeds under engine-relevant conditions: uncertainty quantification and minimization in spherically expanding flame experiments, Combust. Flame 163 (2016) 270–283.
[13] P.D. Ronney, Effect of chemistry and transport properties on near-limit flames at microgravity, Combust. Sci. Technol. 59 (1988) 123–141.
[14] V.F. Zakaznov, et al., Determination of normal flame velocity and critical diameter of flame extinction in ammonia-air mixture, Combust., Explos. Shock Waves 14 (1978) 710–713.
[15] U. Pfahl, et al., Flammability limits, ignition energy, and flame speeds in H_2–CH_4–NH_3–N_2O–O_2–N_2 mixtures, Combust. Flame 123 (2000) 140–158.
[16] K. Takizawa, et al., Burning velocity measurements of nitrogen-containing compounds, J. Hazard. Mater. 155 (2008) 144–152.
[17] B. Mei, et al., Experimental and kinetic modeling investigation on the laminar flame propagation of ammonia under oxygen enrichment and elevated pressure conditions, Combust. Flame 210 (2019) 236–246.
[18] Z. Chen, On the accuracy of laminar flame speeds measured from outwardly propagating spherical flames: methane/air at normal temperature and pressure, Combust. Flame 162 (2015) 2442–2453.
[19] F.N. Egolfopoulos, et al., Advances and challenges in laminar flame experiments and implications for combustion chemistry, Prog. Energy Combust. Sci. 43 (2014) 36–67.
[20] J. Santner, et al., High temperature oxidation of formaldehyde and formyl radical: a study of 1,3,5-trioxane laminar burning velocities, Proc. Combust. Inst. 35 (2015) 687–694.
[21] D. Bradley, et al., Burning velocities, Markstein lengths, and flame quenching for spherical methane-air flames: a computational study, Combust. Flame 104 (1996) 176–198.
[22] P.D. Ronney, H.Y. Wachman, Effect of gravity on laminar premixed gas combustion I: flammability limits and burning velocities, Combust. Flame 62 (1985) 107–119.
[23] L. Qiao, et al., Near-limit laminar burning velocities of microgravity premixed hydrogen flames with chemically-passive fire suppressants, Proc. Combust. Inst. 31 (2007) 2701–2709.
[24] D. Bradley, et al., Laminar burning velocities of lean hydrogen–air mixtures at pressures up to 1.0MPa, Combust. Flame 149 (2007) 162–172.
[25] D. Bradley, Instabilities and flame speeds in large-scale premixed gaseous explosions, Philos. Trans. R. Soc. Lond. A: Math., Phys. Eng. Sci. 357 (1999) 3567–3581.
[26] M.P. Burke, et al., Effect of cylindrical confinement on the determination of laminar flame speeds using outwardly propagating flames, Combust. Flame 156 (2009) 771–779.
[27] Z. Chen, Effects of radiation and compression on propagating spherical flames of methane/air mixtures near the lean flammability limit, Combust. Flame 157 (2010) 2267–2276.
[28] F. Wu, et al., Uncertainty in stretch extrapolation of laminar flame speed from expanding spherical flames, Proc. Combust. Inst. 35 (2015) 663–670.
[29] J. Jayachandran, et al., A study of propagation of spherically expanding and counterflow laminar flames using direct measurements and numerical simulations, Proc. Combust. Inst. 35 (2015) 695–702.
[30] Z. Chen, Effects of radiation absorption on spherical flame propagation and radiation-induced uncertainty in laminar flame speed measurement, Proc. Combust. Inst. 36 (2017) 1129–1136.
[31] Z. Chen, Effects of radiation on large-scale spherical flame propagation, Combust. Flame 183 (2017) 66–74.
[32] C.H. Sohn, et al., Effects of radiation on the uncertainty of flame speed determination using spherically propagating flames with $CO/CO_2/H_2O$ dilutions at elevated pressures, Int. J. Heat Mass Transfer 86 (2015) 820–825.
[33] A. Omari, L. Tartakovsky, Measurement of the laminar burning velocity using the confined and unconfined spherical flame methods – a comparative analysis, Combust. Flame 168 (2016) 127–137.
[34] H. Yu, et al., Radiation-induced uncertainty in laminar flame speed measured from propagating spherical flames, Combust. Flame 161 (2014) 2815–2824.
[35] R.R. Burrell, et al., Effects of stretch and thermal radiation on difluoromethane/air burning velocity measurements in constant volume spherically expanding flames, Proc. Combust. Inst. 37 (2019).
[36] H. Nakamura, M. Shindo, Effects of radiation heat loss on laminar premixed ammonia/air flames, Proc. Combust. Inst. 37 (2019) 1741–1748.
[37] R.S. Barlow, et al., Scalar profiles and NO formation in laminar opposed-flow partially premixed methane/air flames, Combust. Flame 127 (2001) 2102–2118.
[38] R.J. Kee, et al., PREMIX: a FORTRAN program for modeling steady laminar one-dimensional premixed flames, Sandia National Laboratories Report, 1985.
[39] S. Zheng, et al., Effects of radiation reabsorption on laminar NH_3/H_2/air flames, Combust. Flame 235 (2022) 111699.
[40] Z. Chen, et al., Studies of radiation absorption on flame speed and flammability limit of CO_2 diluted methane flames at elevated pressures, Proc. Combust. Inst. 31 (2007) 2693–2700.
[41] Y. Ju, et al., Effects of radiative emission and absorption on the propagation and extinction of premixed gas flames, Symp. Int. Combust. Proc. 27 (1998) 2619–2626.
[42] M. Ilbas, The effect of thermal radiation and radiation models on hydrogen–hydrocarbon combustion modelling, Int. J. Hydrogen Energy 30 (2005) 1113–1126.
[43] T. Daguse, et al., Study of radiative effects on laminar counterflow H_2/O_2N_2 diffusion flames, Combust. Flame 106 (1996) 271–287.
[44] Z. Chen, et al., Effects of Lewis number and ignition energy on the determination of laminar flame speed using propagating spherical flames, Proc. Combust. Inst. 32 (2009) 1253–1260.
[45] P. Dai, Z. Chen, Supersonic reaction front propagation initiated by a hot spot in n-heptane/air mixture with multistage ignition, Combust. Flame 162 (2015) 4183–4193.
[46] M. Faghih, Z. Chen, Two-stage heat release in nitromethane/air flame and its impact on laminar flame speed measurement, Combust. Flame 183 (2017) 157–165.
[47] Z. Chen, et al., Effects of compression and stretch on the determination of laminar flame speeds using propagating spherical flames, Combust. Theor. Model. 13 (2009) 343–364.
[48] R.J. Kee, et al., CHEMKIN-II: a FORTRAN chemical kinetics package for the analysis of gas-phase chemical kinetics, Sandia Report. SAND89-8009B, (1993).
[49] J. Santner, et al., Uncertainties in interpretation of high pressure spherical flame propagation rates due to thermal radiation, Combust. Flame 161 (2014) 147–153.
[50] M. Faghih, et al., On laminar premixed flame propagating into autoigniting mixtures under engine-relevant conditions, Proc. Combust. Inst. 37 (2019) 4673–4680.
[51] M. Faghih, et al., On the determination of laminar flame speed from low-pressure and super-adiabatic propagating spherical flames, Proc. Combust. Inst. 37 (2019) 1505–1512.
[52] M. Faghih, et al., The explosion characteristics of methane, hydrogen and their mixtures: a computational study, J. Loss Prev. Process Ind. 40 (2016) 131–138.
[53] S. Balusamy, et al., Direct measurement of local instantaneous laminar burning velocity by a new PIV algorithm, Exp. Fluids 50 (2011) 1109–1121.
[54] E. Varea, et al., Measurement of laminar burning velocity and Markstein length relative to fresh gases using a new postprocessing procedure: application to laminar spherical flames for methane, ethanol and isooctane/air mixtures, Combust. Flame 159 (2012) 577–590.
[55] L.S. Rothman, et al., The HITRAN 2008 molecular spectroscopic database, J. Quant. Spectrosc. Radiat. Transfer 110 (2009) 533–572.
[56] Y. Ju, et al., Effects of the Lewis number and radiative heat loss on the bifurcation and extinction of CH_4/O_2-N_2-He flames, J. Fluid Mech. 379 (1999) 165–190.
[57] A. Stagni, et al., An experimental, theoretical and kinetic-modeling study of the gas-phase oxidation of ammonia, React. Chem. Eng. 5 (2020) 696–711.
[58] A. Hayakawa, et al., Laminar burning velocity and Markstein length of ammonia/air premixed flames at various pressures, Fuel 159 (2015) 98–106.
[59] X. Han, et al., Experimental and kinetic modeling study of laminar burning velocities of NH_3/air, NH_3/H_2/air, NH_3/CO/air and NH_3/CH_4/air premixed flames, Combust. Flame 206 (2019) 214–226.
[60] C. Lhuillier, et al., Experimental investigation on laminar burning velocities of ammonia/hydrogen/air mixtures at elevated temperatures, Fuel 263 (2020) 116653.
[61] L. Berger, et al., A DNS study of the impact of gravity on spherically expanding laminar premixed flames, Combust. Flame 216 (2020) 412–425.
[62] Z. Chen, On the extraction of laminar flame speed and Markstein length from outwardly propagating spherical flames, Combust. Flame 158 (2011) 291–300.
[63] E. Varea, et al., Pressure effects on laminar burning velocities and Markstein lengths for isooctane-ethanol-air mixtures, Proc. Combust. Inst. 34 (2013) 735–744.
[64] E. Varea, et al., Determination of burning velocities from spherically expanding H_2/air flames, Proc. Combust. Inst. 35 (2015) 711–719.